ANTIOXIDANTS & REDOX SIGNALING
Volume 21, Number 13, 2014

DOI: 10.1089/ars.2013.5677

ORIGINAL RESEARCH COMMUNICATION

Dual Oxidase 2 in Lung Epithelia Is Essential for Hyperoxia-Induced Acute Lung Injury in Mice

Min-Ji Kim,[1,2] Jae-Chan Ryu,[1,2] Younghee Kwon,[1,2] Suhee Lee,[3] Yun Soo Bae,[3] Joo-Heon Yoon,[1,2,4,5] and Ji-Hwan Ryu[1,2]

Abstract

Aims: Acute lung injury (ALI) induced by excessive hyperoxia has been employed as a model of oxidative stress imitating acute respiratory distress syndrome. Under hyperoxic conditions, overloading quantities of reactive oxygen species (ROS) are generated in both lung epithelial and endothelial cells, leading to ALI. Some NADPH oxidase (NOX) family enzymes are responsible for hyperoxia-induced ROS generation in lung epithelial and endothelial cells. However, the molecular mechanisms of ROS production in type II alveolar epithelial cells (AECs) and ALI induced by hyperoxia are poorly understood. ***Results:*** In this study, we show that dual oxidase 2 (DUOX2) is a key NOX enzyme that affects hyperoxia-induced ROS production, particularly in type II AECs, leading to lung injury. In DUOX2 mutant mice ($DUOX2^{thyd/thyd}$) or mice in which DUOX2 expression is knocked down in the lungs, hyperoxia-induced ALI was significantly lower than in wild-type (WT) mice. DUOX2 was mainly expressed in type II AECs, but not endothelial cells, and hyperoxia-induced ROS production was markedly reduced in primary type II AECs isolated from $DUOX2^{thyd/thyd}$ mice. Furthermore, DUOX2-generated ROS are responsible for caspase-mediated cell death, inducing ERK and JNK phophorylation in type II AECs. ***Innovation:*** To date, no role for DUOX2 has been defined in hyperoxia-mediated ALI despite it being a NOX homologue and major ROS source in lung epithelium. ***Conclusion:*** Here, we present the novel finding that DUOX2-generated ROS induce AEC death, leading to hyperoxia-induced lung injury. *Antioxid. Redox Signal*. 21, 1803–1818.

Introduction

OXYGEN IS GENERALLY ADMINISTERED to patients with significant respiratory and cardiac disease to enhance the delivery of oxygen to peripheral tissues. In premature babies who are deficient in surfactant production from type II alveolar epithelial cells (AECs), treatment with high oxygen concentrations is also demanded (1, 5). However, excessive oxygen for a prolonged period of time causes hyperoxic acute lung injury (ALI) (48). The damage to alveolar cells leads to the collapse of alveolar-capillary barrier integrity, resulting in interstitial edema, a subsequent gas exchange impairment, and mortality (49, 50). Several studies have shown that hyperoxia induces oxidative stress and consequent overproduction of reactive oxygen species (ROS), leading to epithelial and endothelial cell death and ALI (11, 32, 40, 43). Though the role of ROS in hyperoxia-induced cell death has not been completely defined, ROS-induced mitogen-activated protein kinase (MAPK) activation is reported to be involved in hyperoxia-induced cell death in lung epithelial and endothelial cells (10, 41, 51). In addition, ROS-mediated cell death is partially dependent on caspase-mediated signaling pathways during hyperoxia (10, 29).

Hyperoxia-induced ROS can be generated by a range of mitochondrial chain transporter and NADPH oxidase (NOX) enzymes (31, 34). NOX-generated ROS were originally studied in the context of host defense in phagocytic cells (3, 30). However, after identification of several homologues of $NOX2/gp^{91}phox$ [NOX1, NOX3-5, dual oxidase 1 (DUOX1), and DUOX2], the known role of NOX-generated ROS has expanded into diverse cellular events, including cell proliferation, differentiation, apoptosis, and inflammation (4,

[1]Research Center for Natural Human Defense System, Yonsei University College of Medicine, Seoul, South Korea.
[2]Brain Korea 21 PLUS Project for Medical Science, Yonsei University College of Medicine, Seoul, South Korea.
[3]Department of Life Science, Ewha Womans University, Seoul, South Korea.
[4]Department of Otorhinolaryngology and [5]The Airway Mucus Institute, Yonsei University College of Medicine, Seoul, South Korea.

Innovation

Oxygen is generally administered to patients with significant respiratory disease to enhance the delivery of oxygen to peripheral tissues. However, excessive oxygen inevitably causes acute lung injury (ALI). In hyperoxic conditions, overloading quantities of reactive oxygen species (ROS) generated by NADPH oxidase (NOX) family enzymes are responsible for ALI. Before the present study, the function of dual oxidase2 (DUOX2) in hyperoxia-mediated ALI had not been described despite the fact that it is a NOX homologue and a major source of ROS in lung epithelium. Our novel findings regarding the regulation of DUOX2-generated ROS may prove helpful in designing therapies to alleviate hyperoxia-induced ALI during treatment for patients who require supplementary oxygen therapy.

7, 28). Several reports have shown that different NOX isoforms are expressed in various lung cell types, and ROS generated from NOXs play a critical role in hyperoxia-induced ALI (11, 22, 45). In particular, NOX1 is required for hyperoxia-induced lung injury, inducing cell death in lung epithelial and endothelial cells (10). NOX2 and NOX4 participate in hyperoxia-induced damage by inducing cell migration and cell death in lung endothelial cells (13, 35, 36). However, until now, no function of DUOXs has been determined in hyperoxia-mediated ALI despite the fact that they are major NOX homologues and a significant source of ROS in lung epithelium. DUOXs were originally identified from the epithelium of the thyroid gland and are essential in thyroid hormone biosynthesis (8). In addition, DUOXs are expressed in epithelial cells of various tissues, including the airways, alveoli, salivary glands, intestinal tract, and prostate (16–19, 21, 47). Recent studies have focused on the role of DUOX-generated ROS in the regulation of innate immune responses in airway epithelial cells (6, 20, 26, 27, 37, 42). Using DUOX2 mutant mice or mice in which DUOX2 gene expression has been suppressed in lung epithelium, we determined its specific role in the type II AECs that regulate hyperoxia-induced ALI. Our study demonstrates that ROS generated by DUOX2 during hyperoxia causes caspase-mediated cell death and ensuing lung injury by inducing ERK and JNK phosphorylation in type II AECs.

Results

DUOX2 plays a bigger role in hyperoxia-induced ALI than NOX1

To establish a mouse model of hyperoxia-induced ALI, we exposed wild-type (WT) mice to room air or 100% oxygen at different time points, and measured the extent of lung damage. Lung injury was evaluated by quantifying vascular leakage using an extravasation assay and analyzing alveolar permeability by measuring the protein concentration and IgM levels in bronchoalveolar lavage (BAL) fluid. In agreement with previous studies, the degree of lung injury in WT mice increased in a time-dependent manner, reaching its peak at 72 h after oxygen exposure (Fig. 1A–C). To determine the role of DUOX2 in hyperoxia-induced lung injury, we compared the extent of lung injury in $DUOX2^{thyd/thyd}$ mutant mice with that of WT mice. Simultaneously, we compared the extent of hyperoxia-induced ALI in $DUOX2^{thyd/thyd}$ mice with that of NOX1-deficient mice ($NOX1^{-/-}$) to determine which NOX enzyme plays a more prominent role in hyperoxia-induced ALI. NOX1 was selected for a comparison because it, rather than NOX2, has been reported to be responsible for hyperoxia-induced lung injury in mice (10). Though the extent of lung injury in $NOX1^{-/-}$ mice was less than the lung injury in $NOX1^{+/+}$ mice (BAL protein: 25.6%, evans blue dye (EBD) extravasation: 28.0%, BAL IgM: 25.9%), $DUOX2^{thyd/thyd}$ mice (BAL protein: 48.5%, EBD extravasation: 43.5%, BAL IgM: 51.3%) had even less lung injury than $NOX1^{-/-}$ mice (Fig. 1D–F). In addition, fibrin deposition in the alveolar spaces of $DUOX2^{thyd/thyd}$ mice was much lower than that in $NOX1^{-/-}$ mice (Fig. 1G–J). All of the experiments with $DUOX2^{thyd/thyd}$ and $NOX1^{-/-}$ mice were carried out simultaneously under identical conditions with the relevant WT control mice ($DUOX2^{+/+}$ and $NOX1^{+/+}$). We then evaluated the lung inflammation induced by hyperoxia in $NOX1^{-/-}$ and $DUOX2^{thyd/thyd}$ mice. Hyperoxia caused an increase in macrophages (approximately threefold) and neutrophils ($\sim$10-fold) in the BAL fluid of WT mice (Fig. 1K). However, the numbers of hyperoxia-induced macrophages and neutrophils in $NOX1^{-/-}$ and $DUOX2^{thyd/thyd}$ mice were similar to those of $NOX1^{+/+}$ and $DUOX2^{+/+}$ mice, respectively (Fig. 1K). We also examined inflammation on lung sections from $DUOX2^{thyd/thyd}$ and $NOX1^{-/-}$ mice *via* hematoxylin and eosin staining, and showed that hyperoxia-induced inflammation is not affected in $DUOX2^{thyd/thyd}$ or $NOX1^{-/-}$ mice (Supplementary Fig. S1A, B; Supplementary Data are available online at www.liebertpub.com/ars). These results indicate that the role of DUOX2 in hyperoxia-induced lung injury is independent of acute lung inflammation.

DUOX2 is responsible for hyperoxia-induced ROS production in type II AECs

We checked the expression levels of NOX1, NOX2, NOX4, DUOX1, and DUOX2 in $DUOX2^{thyd/thyd}$ mice to determine whether the decrease in hyperoxia-induced lung injury in $DUOX2^{thyd/thyd}$ mice is attributable to down-regulation of other NOX enzymes. There were no critical changes in the expression of NOX1, NOX2, NOX4, DUOX1, or DUOX2 genes in $DUOX2^{thyd/thyd}$ mice exposed to hyperoxia (Fig. 2A). In addition, there were no essential changes in the expression levels of NOX2, NOX4, DUOX1, or DUOX2 in $NOX1^{-/-}$ mice exposed to hyperoxia (Supplementary Fig. S2). The results suggested that expression levels of other NOXs were not affected in $DUOX2^{thyd/thyd}$ or $NOX1^{-/-}$ mice under normal or hyperoxia conditions. To examine the localization of DUOX2 expression, lung sections from WT mice were double stained with either anti-DUOX2 antibody and anti-surfactant protein-c (SP-C) (a type II AEC-specific marker) antibody, or anti-DUOX2 antibody and anti-von Willebrand factor (VWF) (an endothelial cell-specific marker) antibody. As shown in Figure 2B and C, DUOX2 was detected in SP-C-expressing cells, but not in VWF-expressing cells, indicating that DUOX2 is mainly expressed in type II AECs, rather than in endothelial cells. To determine the contribution of DUOX2 to hyperoxia-induced ROS production in primary type II AECs, we first examined the population of primary Type I AECs and Type II AECs

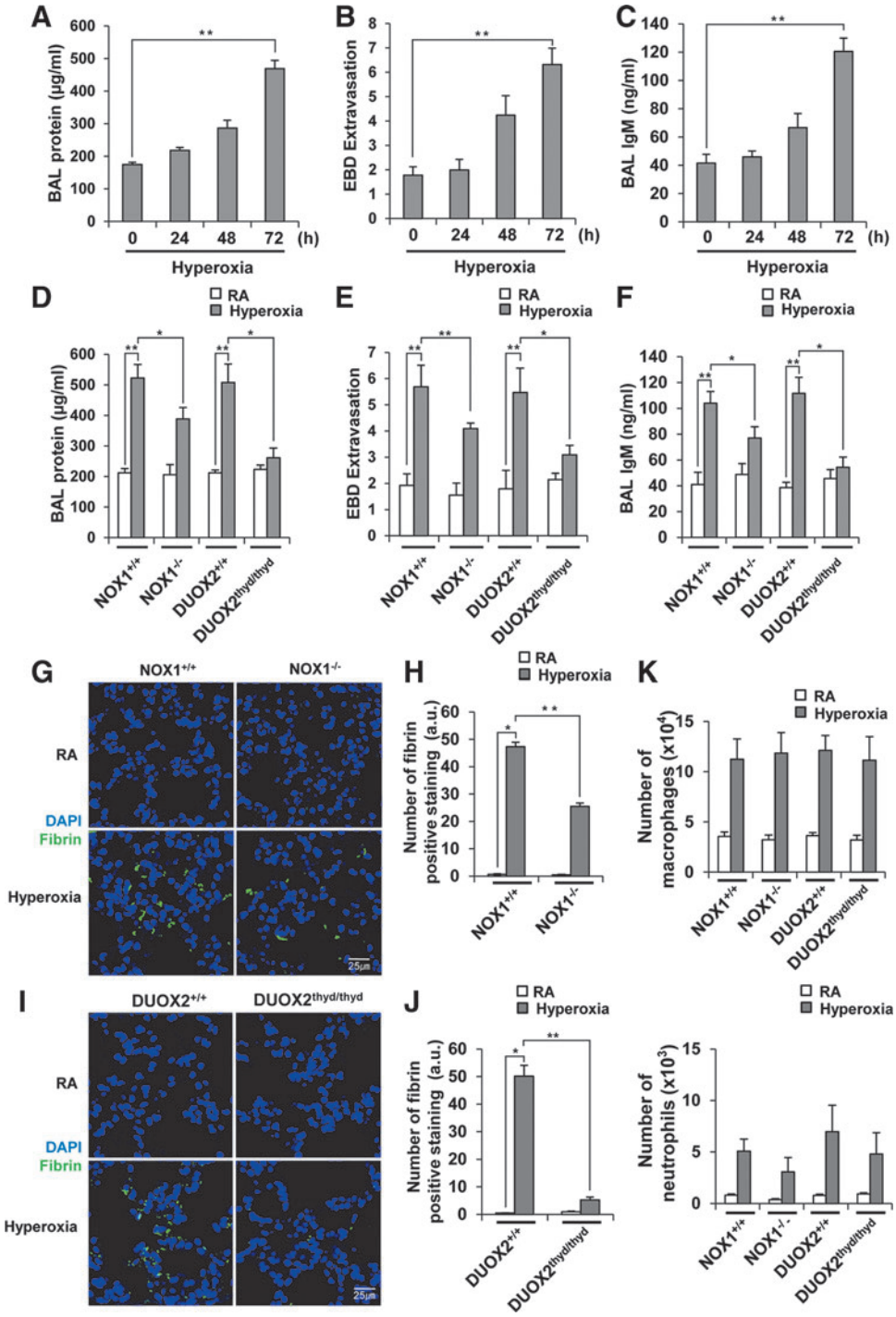

FIG. 1. DUOX2 is critical in hyperoxia-induced ALI in mice. **(A–C)** Wild-type (WT) mice were exposed to hyperoxia for 0, 24, 48, or 72 hrs. **(A)** Bronchoalveolar lavage (BAL) protein, **(B)** Evans blue dye (EBD) extravasation, and **(C)** BAL IgM were measured. **(D–K)** $DUOX2^{thyd/thyd}$ mice, $NOX1^{-/-}$ mice, and their relevant WT control mice ($DUOX2^{+/+}$ and $NOX1^{+/+}$) were exposed to hyperoxia for 72 h. All of the experiments with $DUOX2^{thyd/thyd}$ and $NOX1^{-/-}$ mice were carried out simultaneously under identical conditions. **(D)** BAL protein, **(E)** EBD extravasation, and **(F)** BAL IgM were measured. **(G, I)** Immunohistochemical (IHC) detection of fibrin in paraffin-embedded lung sections. Lung sections were stained with anti-fibrin antibody (*green*) and 4′,6-diamidino-2-phenylindole (DAPI) (*blue*), and were visualized by confocal microscopy. **(K)** Number of neutrophils and macrophages in BAL fluid were counted by staining with a Diff-Quik Stain Set. $*p < 0.05$, $**p < 0.01$. All results are shown as mean ± SEM. The results represent three independent experiments, and three to five mice were used per group.

from WT mice at different time points after hyperoxia exposure *via* FACS analysis. Two days after hyperoxia, 92.2% of the total cells were Type II AECs, and 5.3% of the total cells were Type I AECs (Supplementary Fig. S3). In this condition, we measured ROS production in primary type II AECs from WT mice at different time points after hyperoxia exposure and then compared the values in primary type II AECs from WT or $DUOX2^{thyd/thyd}$ mice utilizing Dichlorodihydrofluorescein (DCF) dye, which is known to be used to mainly detect hydrogen peroxide (H_2O_2). As a positive control, we showed that H_2O_2 treatment into type II AECs from WT mice increased ROS generation (Fig. 3A, B). H_2O_2 production started at 1 day after hyperoxia exposure and was at a maximum 2 days after hyperoxia exposure (Fig. 3A, B). Hyperoxia-induced H_2O_2 production was dramatically decreased in type II AECs from $DUOX2^{thyd/thyd}$ mice (Fig. 3C, D), while it was not affected in type II AECs from $NOX1^{-/-}$ mice (Fig. 3E, F). In contrast, when utilizing Dihydroethidium (DHE) dye, which is known to be used to mainly detect superoxide (O_2^-), hyperoxia-induced O_2^- production was not affected in type II AECs from $DUOX2^{thyd/thyd}$ mice (Supplementary Fig. S4A, B); while it was decreased in type II AECs from $NOX1^{-/-}$ mice (Supplementary Fig. S4C, D). These results suggested that hyperoxia-induced

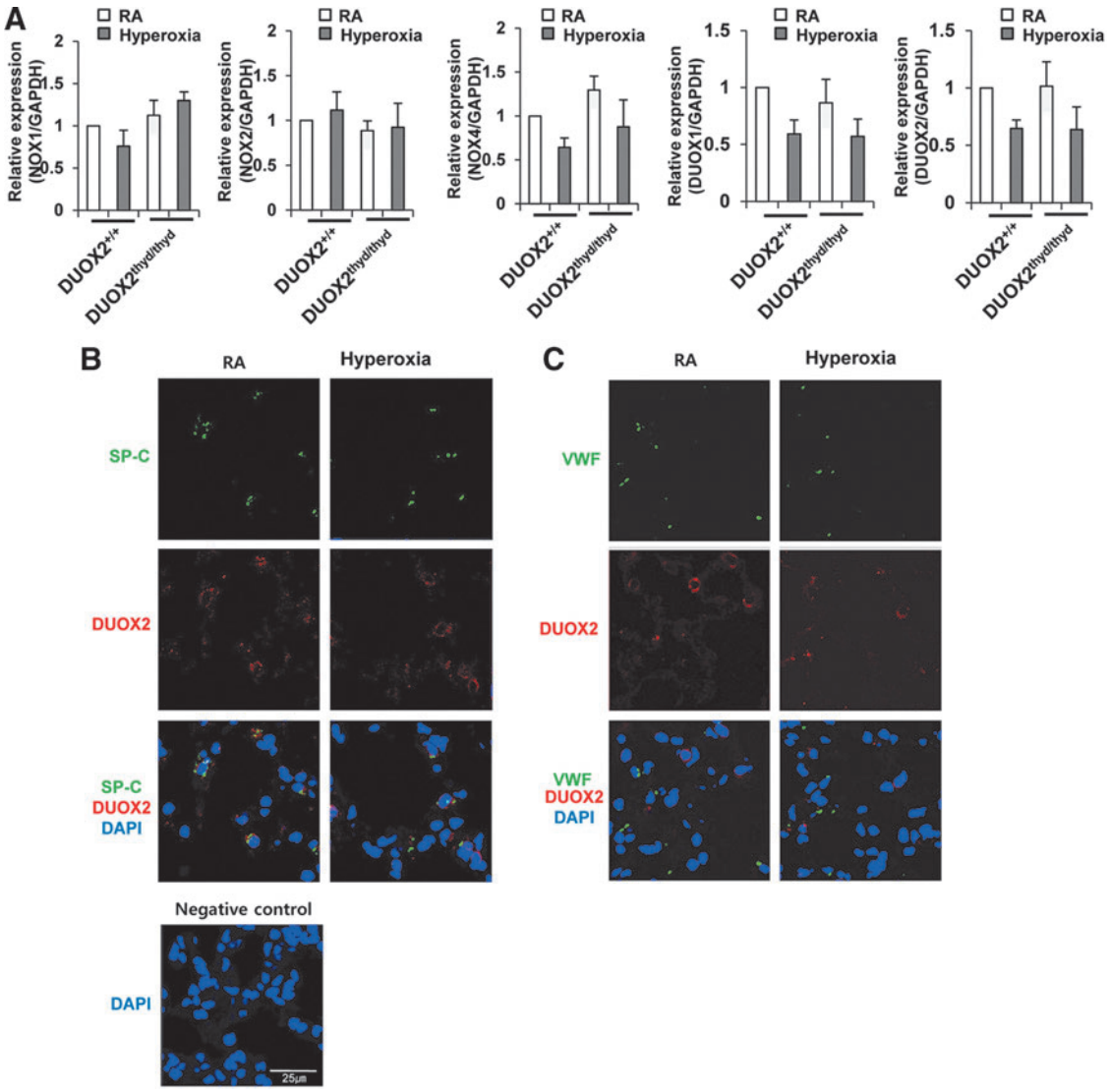

FIG. 2. DUOX2 is mainly expressed in type II alveolar epithelial cells (AECs) in the lungs. (A) Relative gene expressions of NOX1, NOX2, NOX4, DUOX1, and DUOX2 in lung tissue of $DUOX2^{thyd/thyd}$ mice exposed to room air (RA) or hyperoxia for 3 days. The expression levels of NOX1, NOX2, NOX4, DUOX1, and DUOX2 in the lungs of $DUOX2^{+/+}$ mice exposed to room air were arbitrarily set as 1. **(B, C)** Images of lung sections of WT mice exposed to RA or hyperoxia for 3 days, which were stained with anti-DUOX2 antibody (*red*), anti-surfactant protein-c (SP-C) antibody (*green*), or anti-von Willebrand factor (VWF) antibody (*green*), followed by their merged versions. Nuclei were stained with DAPI (*blue*). The negative control shows the IHC detection without any of the anti-DUOX2 antibody, anti-SP-C antibody, and anti-VWF antibody under the same experimental conditions. All results are shown as mean ± SEM. The results represent three independent experiments, and three to five mice were used per group.

H_2O_2 production in type II AECs is mainly mediated by DUOX2, while O_2^- production is primarily mediated by NOX1. To investigate that DUOX2 activation in type II AECs by hyperoxia exposure is caused by an increase in the DUOX2 expression or Ca^{2+} signaling or both, we first examined the mRNA expression and protein expression of DUOX2 in response to hyperoxia. The protein expression of DUOX2 was increased by hyperoxia for 2 days (Fig. 3G), whereas the mRNA expression level was not increased under the same conditions (Supplementary Fig. S5), suggesting that upregulation of protein levels of DUOX2 by hyperoxia might be controlled by post-transcriptional modifications, rather than regulation of transcriptional levels. We next measured the hyperoxia-induced ROS generation in type II AECs pretreated with Ca^{2+} signaling inhibitor (BAPTA-AM). Hyperoxia-induced ROS generation was decreased by Ca^{2+} signaling inhibitor in type II AECs (Fig. 3H). These results indicated that both the increase of DUOX2 expression and the activation of Ca^{2+} signaling are required for hyperoxia-induced ROS generation in type II AECs.

DUOX2 is required for hyperoxia-induced cell death in lung type II AECs

To investigate the role of DUOX2 in hyperoxia-induced cell death in lung epithelia, we examined BAL lactate

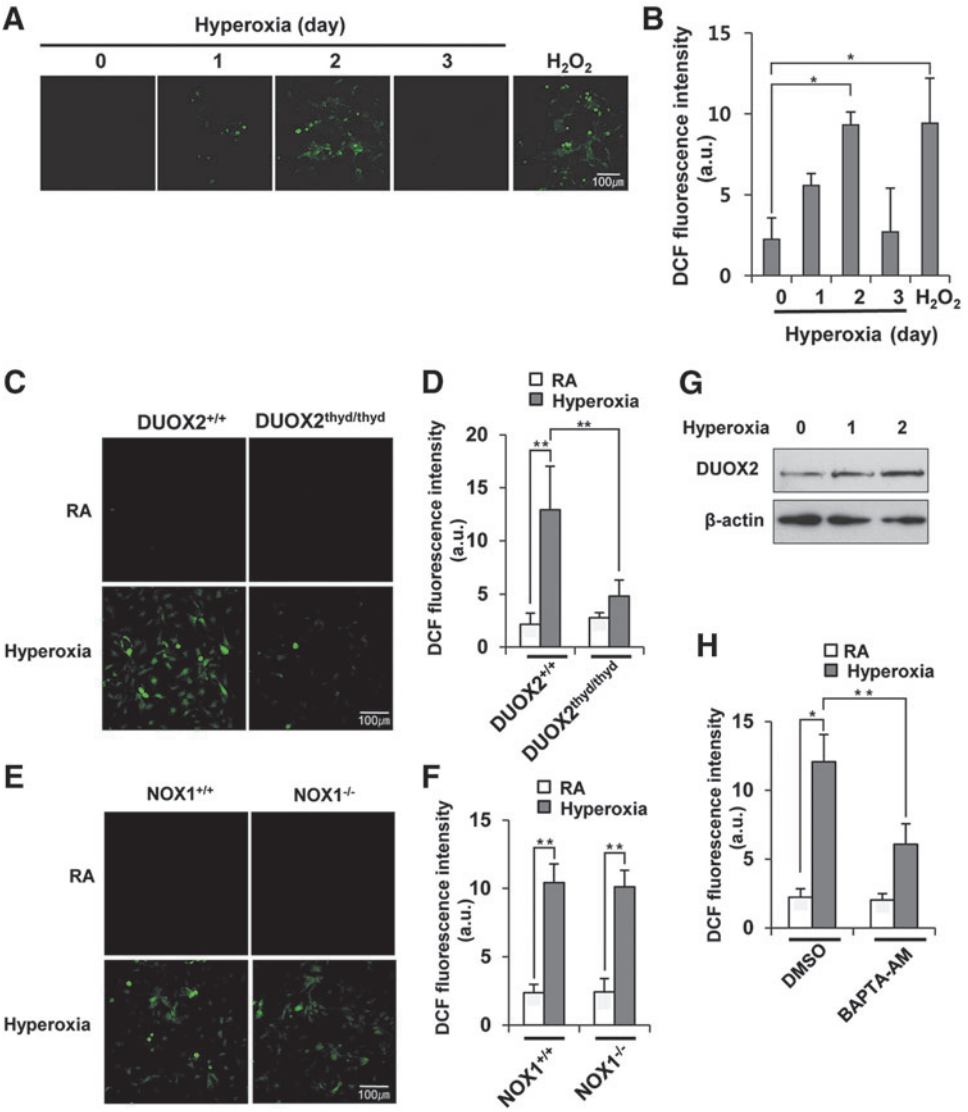

FIG. 3. DUOX2 is responsible for hyperoxia-induced H_2O_2 production in type II AECs. **(A, B)** Type II AECs isolated from WT mice were exposed to hyperoxia for 0, 1, 2, or 3 days, followed by 10 min of incubation with 2′,7′-dichlorohydrofluorescin diacetate (DCF-DA). **(A)** DCF fluorescence intensity was observed by a confocal microscope and **(B)** quantified by densitometric analysis. **(C–F)** Type II AECs isolated from $DUOX2^{thyd/thyd}$ or $NOX1^{-/-}$ mice were exposed to RA or hyperoxia for 2 days. **(C, E)** DCF fluorescence intensity was observed by a confocal microscope and **(D, F)** quantified by densitometric analysis. **(G)** DUOX2 proteins were detected in Type II AECs that were exposed to hyperoxia for 0, 1, or 2 days. **(H)** Quantification of hyperoxia-induced DCF fluorescence intensity in Type II AECs pretreated with BAPTA-AM. $*p < 0.05$, $**p < 0.01$. All results are shown as mean ± SEM. The results represent three independent experiments, and three to five mice were used per group.

dehydrogenase (LDH) release, an indicator of cell death, in $DUOX2^{thyd/thyd}$ mice during hyperoxia. BAL LDH release induced by hyperoxia was dramatically decreased in $DUOX2^{thyd/thyd}$ mice (Fig. 4A). Though the extent of LDH release in $NOX1^{-/-}$ mice is lower than in $NOX1^{+/+}$ mice (21.4%), the decrease seen in $DUOX2^{thyd/thyd}$ mice (47.6%) was larger than that in $NOX1^{-/-}$ mice (Fig. 4A). These observations are in agreement with previous data (Fig. 1D–J). We hypothesized that the decrease in the cell death in $DUOX2^{thyd/thyd}$ mice lung by hyperoxia exposure was caused by cell death in type II AECs, because DUOX2 is responsible for hyperoxia-induced ROS production in type II AECs and ROS-dependent caspase3 activation in lung epithelium participates in hyperoxia-induced cell death (10, 51). To verify this, we double stained lung sections from WT or $DUOX2^{thyd/thyd}$ mice *in situ* with anti-SP-C antibody and TUNEL, or anti-SP-C antibody and anti-cleaved caspase3 antibody. Double-stained cells with anti-SP-C antibody and TUNEL (Fig. 4B, C), as well as with anti-SP-C antibody and anti-cleaved caspase3 antibody (Fig. 4F, G), were dramatically decreased in $DUOX2^{thyd/thyd}$ mice by hyperoxia exposure. Double-stained cells with anti-SP-C antibody and TUNEL (Fig. 4D, E), as well as with anti-SP-C antibody and anti-cleaved caspase3 antibody (Fig. 4H, I), were also decreased in $NOX1^{-/-}$ mice, though the extent of decline was less than that of $DUOX2^{thyd/thyd}$ mice. We also showed that cleaved PARP-1 induced by hyperoxia was decreased in lung lysates in $DUOX2^{thyd/thyd}$ and $NOX1^{-/-}$ mice, respectively (Fig. 4J, K). These results indicated that DUOX2 is mainly responsible for hyperoxia-induced cell death in lung type II AECs.

DUOX2 is responsible for hyperoxia-induced ERK and JNK phosphorylation in lung epithelium

Since MAPK phosphorylation has been reported to be responsible for hyperoxia-induced cell death (10, 51), we investigated the role of DUOX2 in the hyperoxia-induced activation of MAPK. Of the MAPK-related proteins tested, JNK and ERK were strongly phosphorylated by hyperoxia exposure (Fig. 5A), while p38 was not (data not shown). Hyperoxia-induced JNK and ERK phosphorylation was

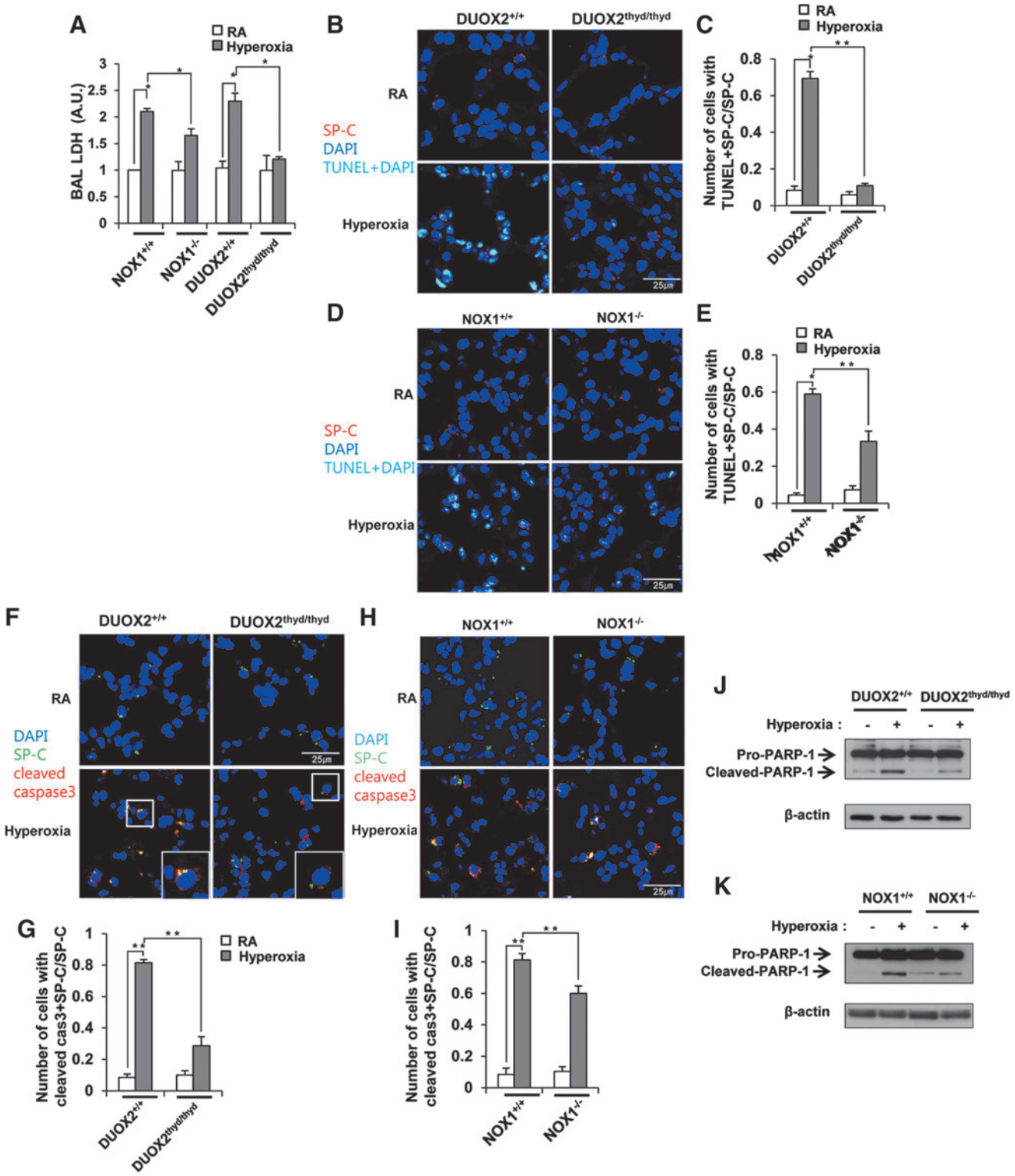

FIG. 4. DUOX2 is required for hyperoxia-induced cell death in type II AECs. **(A–K)** DUOX2$^{thyd/thyd}$, NOX1$^{-/-}$ mice, and their relevant WT control mice (DUOX2$^{+/+}$ and NOX1$^{+/+}$) were exposed to RA or hyperoxia for 3 days. **(A)** Lactate dehydrogenase (LDH) activity from BAL fluid was measured. **(B, D)** Merged images of lung sections, each stained with anti-SP-C antibody (*red*), terminal deoxynucleotidyl transferase (TdT)-mediated dUTP nick end labeling (TUNEL) (*green*), DAPI (*blue*), and TUNEL with DAPI (*sky blue*). **(C, E)** Quantification of cells with TUNEL + SP-C/SP-C in **(B)** and **(D)**, respectively. **(F, H)** Merged images of lung sections, each stained with anti-SP-C antibody (*green*), anti-cleaved caspase3 antibody (*red*), and DAPI (blue). **(G, I)** Quantification of cells with cleaved caspase3 + SP-C/SP-C in **(F)** and **(H)**, respectively. **(J, K)** Cleaved PARP-1 proteins were detected in lung lysates. $*p < 0.05$, $**p < 0.01$. All results are shown as mean ± SEM. The results represent three independent experiments, and three to five mice were used per group.

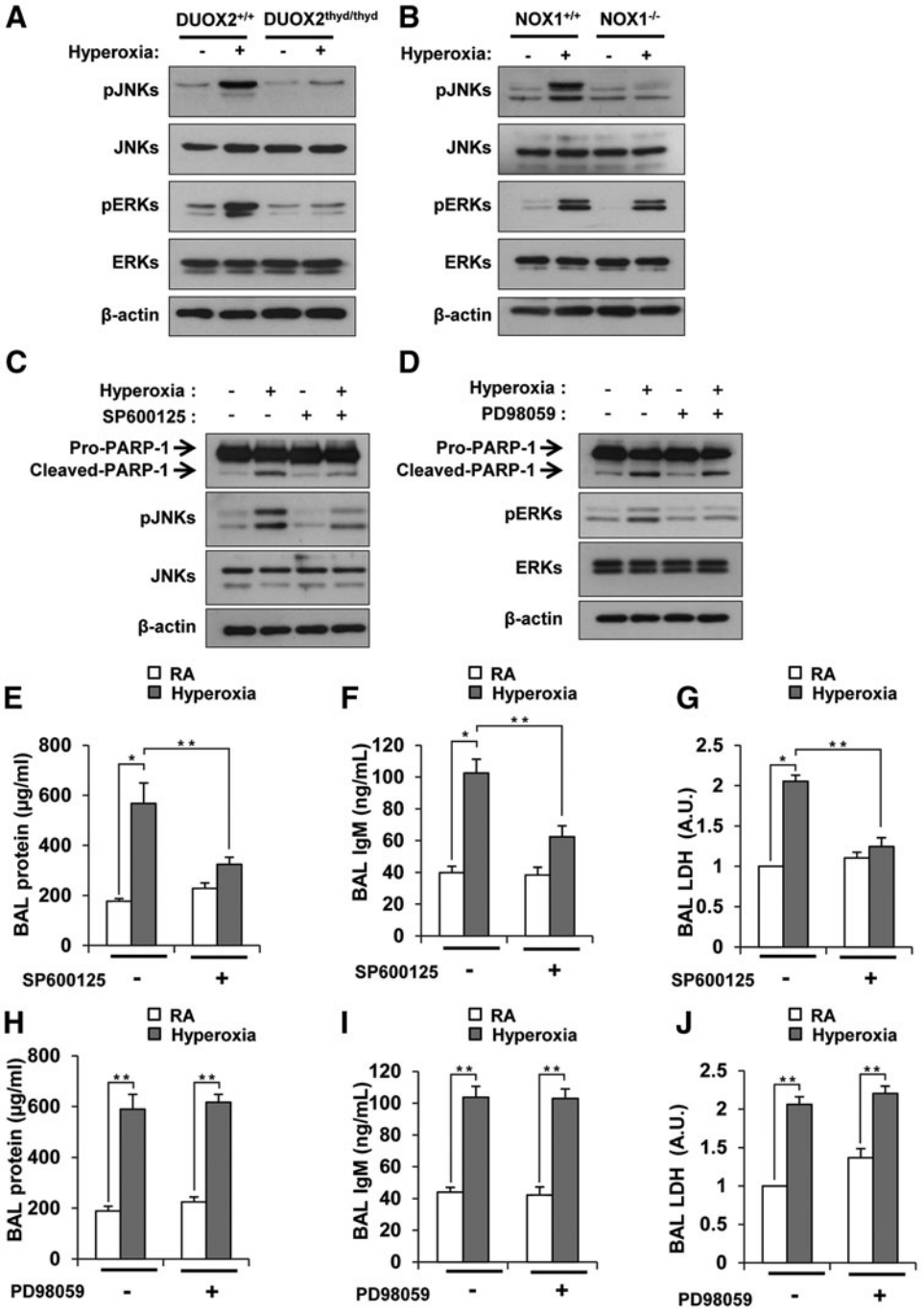

FIG. 5. DUOX2 is responsible for ERK and JNK phosphorylation in mouse lung during hyperoxia. (A, B) $DUOX2^{thyd/thyd}$, $NOX1^{-/-}$ mice, and their relevant WT control mice ($DUOX2^{+/+}$ and $NOX1^{+/+}$) were exposed to RA or hyperoxia for 3 days. Detction of phosphorylated JNKs (pJNKs), phosphorylated ERKs (pERKs), total JNKs, and total ERKs in lung lysates. **(C)** Detection of hyperoxia-induced cleaved PARP-1 and p-JNK in MLE12 cells pretreated with SP600125. **(D)** Detection of hyperoxia-induced cleaved PARP-1 and p-ERK in MLE12 cells pretreated with PD98059. **(E–G)** WT mice pretreated with SP600125 were exposed to RA or hyperoxia for 3 days. **(E)** BAL protein, **(F)** BAL IgM, and **(G)** BAL LDH were measured. **(H–J)** WT mice pretreated with PD98059 were exposed to RA or hyperoxia for 3 days. **(H)** BAL protein, **(I)** BAL IgM, and **(J)** BAL LDH were measured. $*p < 0.05$, $**p < 0.01$. All results are shown as mean ± SEM. The results represent three independent experiments, and three to five mice were used per group.

lower in $DUOX2^{thyd/thyd}$ mice than in WT mice (Fig. 5A); while JNK phosphorylation, but not ERK phosphorylation, was lower in $NOX1^{-/-}$ mice by hyperoxia exposure (Fig. 5B). These results indicated that hyperoxia-induced JNK activation is dependent on both DUOX2 and NOX1, but hyperoxia-induced ERK activation is dependent on DUOX2, but not on NOX1. To verify the effect of JNK and ERK activation on hyperoxia-induced cell death in type II AECs, we examined the hyperoxia-induced PARP-1 cleavage in murine transformed lung epithelial 12 (MLE12) cells pretreated with SP600125, a JNK inhibitor, and PD98059, an ERK inhibitor. Hyperoxia-induced PARP-1 cleavage was decreased by SP600125 treatment (Fig. 5C), whereas it was not decreased by PD98059 (Fig. 5D). Consistent with the data in MLE12 cells, hyperoxia-induced lung injuries were decreased in WT mice pretreated with SP600125 (Fig. 5E–G); while they were not decreased in those pretreated with PD98059 (Fig. 5H–J), indicating that JNK activation, rather than ERK activation, induces hyperoxia-induced cell death and lung injury. Together, these results demonstrated that DUOX2-induced cell death and lung injury by hyperoxia is mediated by JNK activation, though DUOX2 mediates activation of both JNK and ERK in response to hyperoxia exposure.

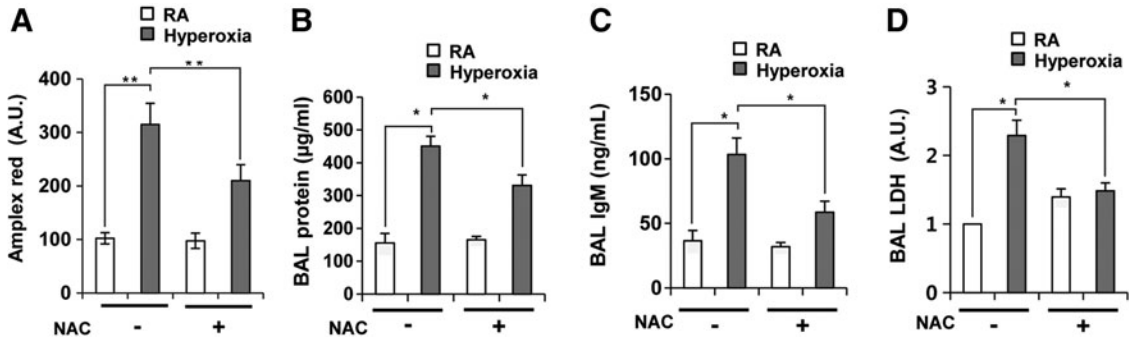

FIG. 6. Hyperoxia-induced ROS generation in lung epithelia is required for acute lung injury. WT mice were intranasally challenged with N-acetylcysteine (NAC), followed by RA or hyperoxia for 3 days. **(A)** H_2O_2 in lung lysates, **(B)** BAL protein, **(C)** BAL IgM, and **(D)** BAL LDH were measured. $*p < 0.05$, $**p < 0.01$. All results are shown as mean ± SEM. The results represent three independent experiments, and three to five mice were used per group.

Hyperoxia-induced ROS generation in lung epithelium is required for ALI

Since hyperoxia-induced H_2O_2 production and cell death were decreased in primary type II AECs from DUOX2$^{thyd/thyd}$ mice (Figs. 3C, D and 4B, C, F, G), we tested whether DUOX2-mediated H_2O_2 in mouse lung epithelium contributes significantly to hyperoxia-induced lung injury. We pretreated lung epithelium from WT mice with N-acetylcysteine (NAC), an ROS-scavenging chemical, and measured ROS production and hyperoxia-induced lung injuries. NAC treatment decreased ROS production (Fig. 6A), BAL protein (Fig. 6B), BAL IgM (Fig. 6C), and BAL LDH (Fig. 6D) in response to hyperoxia. As a positive control, we demonstrated that H_2O_2 treatment into mouse lung increased ROS generation in lung epithelium (Supplementary Fig. S6). These results suggest that hyperoxia-generated ROS in lung epithelium play an important role in hyperoxia-induced ALI

DUOX2, but not DUOX1, is responsible for hyperoxia-induced cell death in type II AECs

To determine which DUOX enzyme is more important in hyperoxia-induced H_2O_2 generation, we first measured H_2O_2 production in MLE12 cells at different time points after hyperoxia exposure. In contrast to primary mouse type II AECs, H_2O_2 generation in MLE12 cells started at 15 min after hyperoxia exposure and peaked at 30 min (Fig. 7A, B). In addition, hyperoxia-induced H_2O_2 generation was decreased by Ca^{2+} signaling inhibitor in MLE12 cells, indicating that hyperoxia-induced Ca^{2+} signaling is required for H_2O_2 generation in MLE12 cells (Supplementary Fig. S7). To specifically suppress the gene expression of DUOX1 and DUOX2 in MLE12 cells, we selected the most specific and effective suppressors of DUOX1 (siDUOX1-5) and DUOX2 (siDUOX2-4) from five candidate duplex siRNAs for each enzyme (Supplementary Fig. S8A, B). During hyperoxia, siDUOX1-5 treatment decreased the expression of DUOX1, but not DUOX2; whereas siDUOX2-4 treatment decreased the expression of DUOX2, but not DUOX1 (Fig. 7C). Suppression of DUOX2 expression dramatically decreased H_2O_2 generation induced by hyperoxia exposure, whereas suppression of DUOX1 had no effect (Fig. 7D). These results indicate that DUOX2, but not DUOX1, is required for hyperoxia-induced H_2O_2 production in type II AECs. Consistent with data obtained from the lung tissue of DUOX2$^{thyd/thyd}$ mice (Figs. 4J and 5A), suppression of DUOX2 expression in MLE12 cells decreased phosphorylation of JNK and ERK, PARP1 cleavage (Fig. 7F), cleaved caspase3 (Fig. 7H, I), and Annexin V staining (Fig. 7J). To confirm the effect of siDUOX2 on hyperoxia-induced cell death, we used a shRNA lentivirus gene suppression system. From the five candidates for each of shDUOX1 and shDUOX, we selected one duplex shDUOX1 (shDUOX1-3) and one shDUOX2 (shDUOX2-3) that most greatly decreased the expression of DUOX1 and DUOX2, respectively (Supplementary Fig. S9A, B). We also showed that the protein level of DUOX2 was decreased in DUOX2-knocked-down cells, but not in DUOX1-knocked-down cells, compared with shcont cells (Supplementary Fig. S10). Consistent with the siDUOX2 data, suppression of DUOX2 expression by treatment with DUOX2 shRNA lentivirus particles decreased H_2O_2 generation (Fig. 7E), ERK and JNK phosphorylation, and PARP-1 cleavage (Fig. 7G) in response to hyperoxia. To confirm the effect of DUOX2 on hyperoxia-induced H_2O_2 production in MLE12 cells, we examined hyperoxia-induced H_2O_2 production in DUOX2-knocked-down cells and DUOX2 overexpressed cells in DUOX2-knocked-down MLE12 cells. Hyperoxia-induced H_2O_2 production was decreased in DUOX2-knocked-down cells, and this decrease was rescued to the level of the control cells by hyperoxia in DUOX2 overexpressed cells in DUOX2-knocked-down cells (Fig. 8A, B). However, hyperoxia-induced H_2O_2 production was not decreased in NOX1-knocked-down cells (Fig. 8A, B). These results were previously confirmed by our results which showed that hyperoxia-induced H_2O_2 production is not decreased in type II AECs from NOX1$^{-/-}$ mice (Fig. 3E, F). To investigate the effect of overexpressed DUOX2 on hyperoxia-induced MAPK activation and cell death, we examined JNK and ERK activation, cleaved caspase3, and cell death by FACS analysis in DUOX2-trasnfected MLE12 cells. Activation of JNK, ERK, and cleaved caspse3 (Fig. 8C), as well as staining of cleaved caspase3 (Fig. 8D, E) and Annexin V (Fig. 8F) was further augmented in DUOX2 overexpressed cells by hyperoxia exposure. These results demonstrated that DUOX2-generated H_2O_2 in MLE12 cells activate hyperoxia-stimulated cell death.

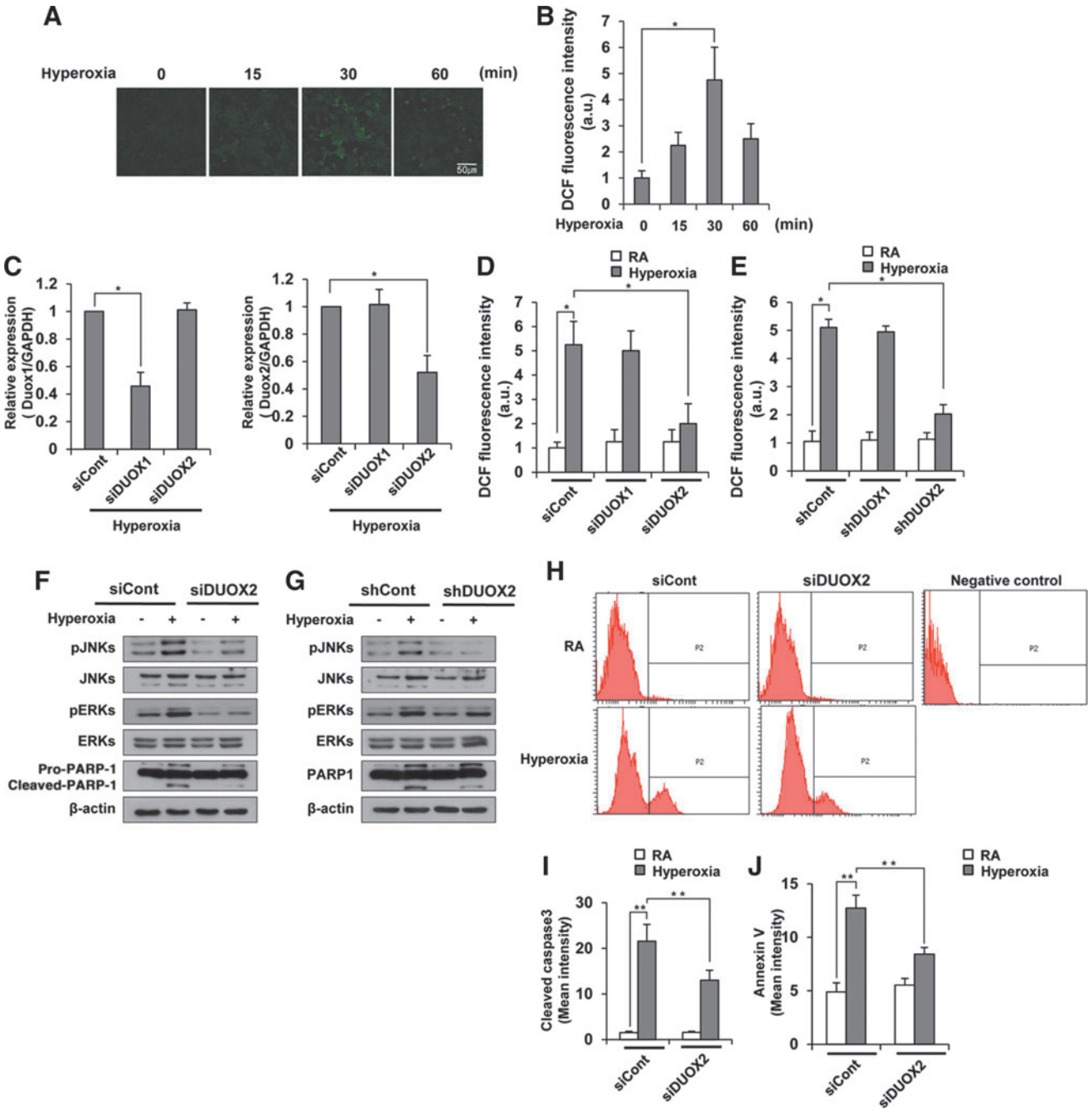

FIG. 7. Hyperoxia-induced cell death in type II AECs is dependent on DUOX2-generated H_2O_2, but not on DUOX1 activity. **(A, B)** Murine transformed lung epithelial 12 (MLE12) cells were exposed to hyperoxia for 0, 15, 30, and 60 min, followed by 10 min of incubation with DCF-DA. **(A)** DCF fluorescence intensity was observed by a confocal microscope and **(B)** quantified by densitometric analysis. **(C)** Relative gene expression of DUOX1 and DUOX2 in MLE12 cells transfected with sicontrol (siCont), siDUOX1, and siDUOX2, respectively. **(D)** Quantification of H_2O_2 production for 30 min after hyperoxia in MLE12 cells transfected with siCont, siDUOX1, and siDUOX2, respectively. **(E)** Quantification of H_2O_2 production for 30 min after hyperoxia in MLE12 cells transfected with scrambled Cont shRNA-containing lentivirus particles (shCont), DUOX1 shRNA-containing lentivirus particles (shDUOX1), and DUOX2 shRNA-containing lentivirus particles (shDUOX2), respectively. **(F)** Detection of pJNKs, pERKs, and cleaved PARP-1 in MLE12 cells transfected with siCont and siDUOX2. **(G)** Detection of pJNKs, pERKs, and cleavage PARP-1 in MLE12 cells transfected with shCont and shDUOX2. **(H)** FACS analysis of MLE12 cells transfected with siCont and siDUOX2 utilizing anti-cleaved caspase3 antibody. **(I)** Mean intensity of cleaved caspase3 in **(H)**. **(J)** Mean intensity of Annexin V from FACS analysis utilizing Annexin V staining in MLE12 cells transfected with siCont and siDUOX2 $*p < 0.05$, $**p < 0.01$. All results are shown as mean ± SEM. The results represent three independent experiments, and three to five mice were used per group.

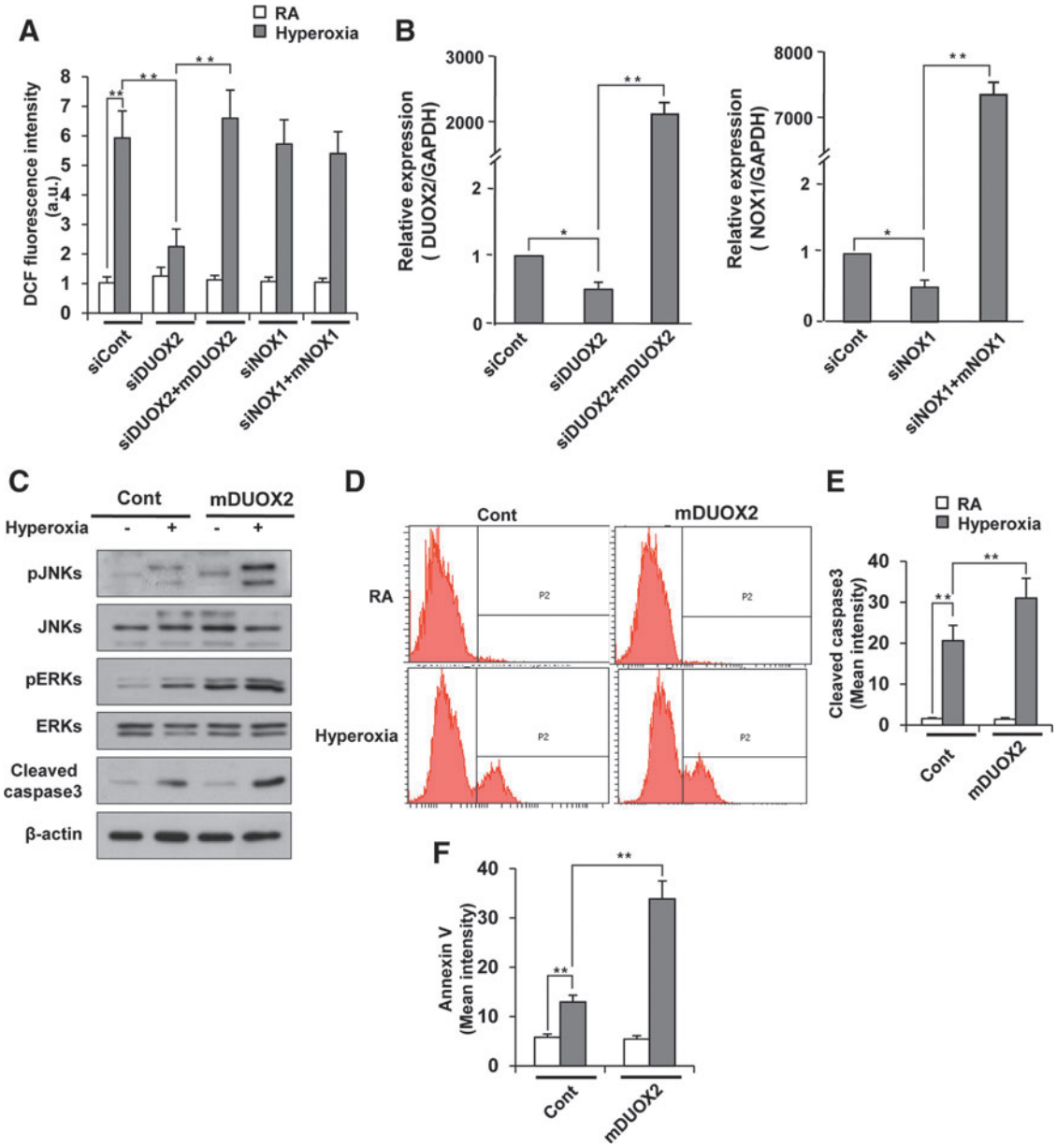

FIG. 8. Hyperoxia-induced cell death in type II AECs is augmented by DUOX2 overexpression. **(A)** Quantification of DCF fluorescence intensity in MLE12 cells transfected with siDUOX2, siDUOX2 and mouse DUOX2 construct (mDUOX2), and siNOX1, as well as siNOX1 and mouse NOX1 construct (mNOX1). **(B)** Relative gene expression of DUOX2 in MLE12 cells transfected with either siDUOX2 or siDUOX2 and mDUOX2. Relative gene expression of NOX1 in MLE12 cells transfected with either siNOX1 or siNOX1 and mNOX1. Gene expression of DUOX2 or NOX1 in MLE12 cells transfected with siCont was arbitrarily set as 1. **(C)** Detection of pJNKs, pERKs, and cleaved caspase3 in MLE12 cells transfected with mDUOX2. **(D)** FACS analysis of MLE12 cells transfected with mDUOX2 utilizing anti-SP-C antibody and anti-cleaved caspase3 antibody. **(E)** Mean intensity of cleaved caspase3 in **(D)**. **(F)** Mean intensity of Annexin V from FACS analysis utilizing anti-SP-C antibody and Annexin V staining in MLE12 cells transfected with mDUOX2. $*p < 0.05$, $**p < 0.01$. All results are shown as mean ± SEM. The results represent three independent experiments, and three to five mice were used per group.

DUOX2 in lung epithelia is required for hyperoxia-induced lung injury

We also tested whether a transient decrease in DUOX2 expression in WT mouse lung epithelia has the same effect as the genetic lack of functional DUOX2 protein in DUOX2$^{thyd/thyd}$ mice. We pretreated the lung epithelia with DUOX2 shRNA lentivirus particles by intranasal challenge, and measured hyperoxia-induced lung injury. Suppression of DUOX2 expression in lung epithelia decreased H_2O_2 production (Fig. 9A), BAL protein (Fig. 9B), BAL IgM (Fig. 9C), and BAL LDH (Fig. 9D). In addition, hyperoxia-induced phosphorylation of JNK and ERK significantly decreased in lung epithelium pretreated with DUOX2 shRNA particles (Fig. 9E).

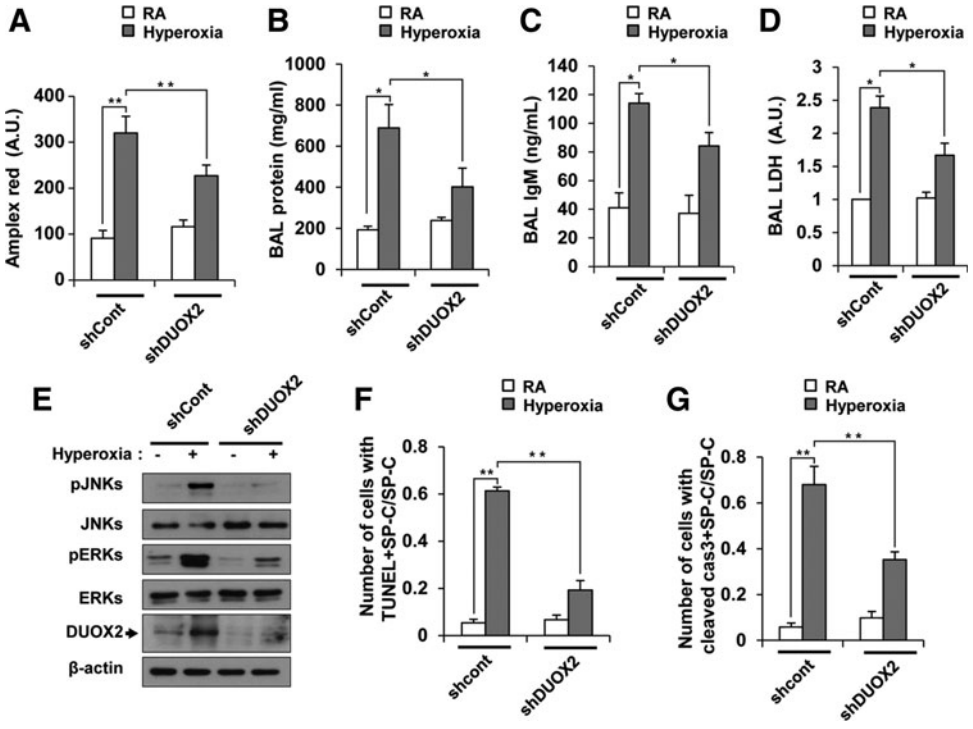

FIG. 9. DUOX2 in lung epithelia is required for hyperoxia-induced lung injury. (A–D) Lung epithelia of WT mice were pretreated with shCont or shDUOX2 lentivirus particles for 6 days, followed by exposure to RA or hyperoxia for 3 days. **(A)** H_2O_2 in lung lysates, **(B)** BAL protein, **(C)** BAL IgM, and **(D)** BAL LDH were measured. **(E)** Detection of pJNKs, pERKs, and DUOX2 in lung lysates. **(F)** Quantification of cells with TUNEL + SP-C/SP-C in lung sections using the same method as in Figure 4B. **(G)** Quantification of cells with cleaved caspase3 + SP-C/SP-C in lung sections using the same methods as in Figure 4F. $*p < 0.05$, $**p < 0.01$. All results are shown as mean ± SEM. The results represent three independent experiments, and three to five mice were used per group.

We also investigated hyperoxia-induced lung injury and MAPK activation in NOX1-knocked-down mice that were pretreated with lentivirus particles with shNOX1 (shNOX1 mice). Expression level of NOX1 was decreased in shNOX1 mice (Supplementary Fig. S11A). H_2O_2 production, lung injuries, including BAL protein, BAL IgM, and BAL LDH (Supplementary Fig. S11B–E), as well as activation of JNK and ERK (Supplementary Fig. S11F) were not decreased in shNOX1 mice, which was different from the results in $NOX1^{-/-}$ mice (Figs. 1D–F and 5B). These results suggested that a decrease in NOX1 expression in shNOX1 mice might not be enough to decrease lung injuries and MAPK activation. In contrast, lung injuries and MAPK activation were decreased in shDUOX2 mice (Fig. 9B–E). To verify the effect of DUOX2 on cell death *in situ*, we double stained lung sections from shcont and shDUOX2 mice with anti-SP-C antibody and TUNEL or anti-SP-C antibody and anti-cleaved caspase3 antibody. Double-stained cells with anti-SP-C antibody and TUNEL (Fig. 9F), as well as with anti-SP-C antibody and anti-cleaved caspase3 antibody (Fig. 9G) were decreased in shDUOX2 mice. Specific suppression of DUOX2 expression in lung epithelium had a similar effect as the lack of a functional DUOX2 protein seen in $DUOX2^{thyd/thyd}$ mice, indicating that DUOX2 is a critical enzyme that regulates the lung epithelial response to hyperoxia and participates in ALI.

Discussion

In this study, we clearly demonstrated that DUOX2 is critical for hyperoxia-induced ALI, and that it increases ROS generation and subsequent cell death in AECs. This was done by showing that increased cell death and ALI caused by hyperoxia were decreased in both mutant mice that are devoid of DUOX2 activity ($DUOX2^{thyd/thyd}$) and mice in which DUOX2 gene expression was knocked down in the lungs. In hyperoxia-induced cell damage, different NOX enzymes, including NOX1, NOX2, and NOX4, play an essential role by generating ROS in alveolar cells (10, 13, 34–36, 44, 46, 51). With regard to NOX2, debatable studies have been reported, with regard to its role in lung injury by hyperoxia. It has been shown that hyperoxia-induced lung injuries, including pulmonary edema and inflammatory responses, are attenuated in $NOX2^{-/-}$ mice (35); whereas another report showed that lung injuries such as alveolar cell death and vascular leakage are not affected in $NOX2^{-/-}$ mice (10). Reflecting on these contrasting reports, it was suggested that NOX2 does not mediate hyperoxia-induced alveolar-capillary disruption, though it is involved in hyperoxia-induced lung inflammation, including infiltration of macrophages and neutrophils. Though both lung epithelial cell and endothelial cells are critical for maintaining alveolar-capillary barrier homeostasis in response to hyperoxia, many studies about the role of NOX in hyperoxia-induced cell damage have been focused on endothelial cells. However, it has recently been shown that NOX1 plays a pivotal role in hyperoxia-induced ALI by increasing ROS generation and cell death in epithelial and endothelial cells (10). Since DUOX2 is mainly expressed in lung epithelial cells and DUOX2-mediated ROS are essential for regulation of cell signaling in response to various stimuli, we compared the level of hyperoxia-induced ALI in $DUOX2^{thyd/thyd}$ mice with that in $NOX1^{-/-}$ mice. Indeed, hyperoxia-induced cell death and ALI were partially attenuated in $NOX1^{-/-}$ mice compared with $NOX1^{+/+}$ mice, and the decrease thereof in $DUOX2^{thyd/thyd}$ mice was much greater than that in $NOX1^{-/-}$ mice. ROS generation and phosphorylation of ERK and JNK in response to hyperoxia in NOX1-suppressed MLE12 cells were not significantly

decreased compared with those in DUOX2-suppressed MLE12 cells (data not shown). Given that NOX-generated ROS induce hyperoxia-stimulated phosphorylation of ERK and cell death in MLE12 cells (51), our experiments suggest that DUOX2-generated ROS, rather than those generated by NOX1, may have a primary role in modulating hyperoxia-induced cell death in lung epithelial cells. In addition, ROS generation was not affected in DUOX1-suppressed MLE12 cells, suggesting that DUOX2 is the main DUOX enzyme responsible for hyperoxia-induced cell signaling in lung epithelial cells.

The accumulation of inflammatory cells caused by hyperoxia was not affected in DUOX2$^{thyd/thyd}$ mice. In agreement with our findings, another study showed that NOX1 and NOX2 are not involved in the lung inflammation caused by hyperoxia (10). It should be noted, however, that these results about the role of NOX in hyperoxia-induced inflammation do not exclude a role for hyperoxia-induced oxidative stress in lung inflammation. NRF2, a transcription factor that induces several antioxidant enzymes and superoxide dismutase, protects the lung against inflammation and hyperoxia-induced ALI (33, 38, 39). Thus, an ROS source other than a NOX enzyme may be required for hyperoxia-induced inflammation. Meanwhile, previous work has demonstrated that DUOX2-generated ROS play an essential role in the innate immune response to bacterial or allergenic challenge in airway epithelial cells, leading to mucosal or allergic inflammation, respectively (6, 12, 17, 20, 23, 26, 27, 37, 42). This suggests that different NOX enzymes may specifically activate distinct signaling pathways by modulating their expression level (10, 35), subcellular localization (7), and interaction with membrane proteins (26, 42) in a signal-dependent manner.

Several lines of evidence showed that purinergic stimulation of lung epithelium increases DUOX-mediated H_2O_2 production, presumably *via* increasing intracellular [Ca^{2+}] and consequent DUOX activation through regulation of its EF-hand domains (2, 19). Although we were unable to detect an increase in intracellular [Ca^{2+}] subsequent to hyperoxia in type II AECs or MLE12 cells, we showed the effect of Ca^{2+} signaling on DUOX2 activation utilizing Ca^{2+} signaling inhibitor (BAPTA AM). We demonstrated that hyperoxia-increased DUOX2 expression and Ca^{2+} signaling are required for ROS generation in type II AECs, while Ca^{2+} signaling, rather than DUOX2 increase, is responsible for ROS generation in MLE12 cells. The difference between type II AECs and MLE12 cells may be caused by the existence of an unknown regulatory system that is capable of rapidly and efficiently activating DUOX2 without an increase in DUOX2 expression in MLR12 cells. The role of DUOX2 in hyperoxia-induced ALI and cell death was demonstrated both in mice genetically lacking functional DUOX2 and in a WT background using a transient DUOX2 suppression system in epithelial cells and mouse lung epithelium. This is imperative from a scientific point of view, as it proves that an acute decrease of DUOX2 expression is sufficient to inhibit ALI and cell death, and the resistance to hyperoxia-induced ALI was not due to chronic adaptation in mutant mice devoid of DUOX2 activity. Inhibition of NOX enzymes was expected to be efficient in hyperoxia-induced ALI, because it inhibits cell death in epithelial and endothelial cells by decreasing oxidative stress from hyperoxia. Moreover, inhibition of NOX4 had been reported to be a potential therapeutic target for ALI through suppression of endothelial cell death (9, 24). However, studies on repressors of hyperoxia-induced ALI *via* inhibition of epithelial cell death are largely unknown.

Our novel findings regarding the regulation of DUOX2-generated ROS in hyperoxia-induced ALI could have a significant effect on therapeutic developments, potentially favoring DUOX2-specific inhibitors mediated oversuppression of epithelial cell death signaling pathways in the treatment of ALI.

Materials and Methods

Mice

DUOX2 mutant mice were purchased from The Jackson Laboratory (25). The recessive *thyd* mutation developed spontaneously in a B6 (129)-*Duox2*^{thyd}/J mouse (Jackson Laboratory; Stock no. 005543). DUOX2$^{+/+}$ littermates were used as wild-type controls. Nox1$^{-/-}$ mice were kindly provided by Dr. Yun Soo Bae (Department of Life Science, Ewha Woman's University, Seoul, Korea). NOX1$^{+/+}$ littermates were used as wild-type controls. All mice used in this study were 8–10 weeks old and maintained in our animal facilities under specific, pathogen-free conditions. All experiments were approved by the Institutional Review Board of Yonsei University College of Medicine.

Hyperoxia exposure

Mice were exposed to hyperoxia in a large AtmosBag (Sigma-Aldrich) that was saturated with almost 100% O_2 at a sufficient flow rate. Control mice were exposed to room air. All mice were allowed free access to water and food. Hyperoxic conditions for cultured cells were achieved by placing type II AECs and MLE 12 cells in a sealed plastic chamber filled with 95% O_2 and 5% CO_2 at 37°C. Controls were placed directly into the cell culture incubator, which was filled with room air supplemented with 5% CO_2, resulting in a final ambient oxygen concentration of 20%.

Antibodies

We purchased antibodies for Western blotting and immunohistochemistry. We used antibodies to ERK (Cell Signaling; #9102), phospho-ERK (Cell Signaling; #9101), JNK (Cell Signaling; #9252), phospho-JNK (Invitrogen; 44-682G), PARP (Cell Signaling; #9542), caspase3 (cell signaling; #9662), and β-actin (Santa Cruz; sc-47778) for Western blotting. We used antibodies to SP-C (Santa Cruz; sc-7706), VWF (Santa Cruz; sc-365712), AQP5 (Santa Cruz; sc-9890), cleaved caspase3 (Cell Signaling; #9661), and fibrin (Dako; A0080) for immunofluorescence. Anti-DUOX2 antibody was kindly provided by Dr. Yun Soo Bae (Department of Life Science, Ewha Woman's University, Seoul, Korea).

Western blot analysis

For Western blots, mouse lung tissues were homogenized with ice-cold RIPA buffer (150 m*M* NaCl, 1.0% NP-40, 0.5% sodium deoxycholate, 0.1% SDS, 50 m*M* Tris, pH 8.0.), protease inhibitor cocktail, and 1 m*M* PMSF. 30 μg of lysate was separated by 8% or 12% SDS-PAGE and transferred to PVDF (Bio-Rad). Membranes were blocked with 5% skim milk in TTBS (Tween-Tris Buffered Saline: 0.5% Tween-20

in 20 *M*m Tris-HCl [pH7.5], 150 *M*m NaCl), and then incubated overnight with primary antibodies and 5% skim milk in TTBS. After washing with TTBS, the blots were incubated with horseradish peroxidase-conjugated secondary antibodies and 5% skim milk in TTBS for 1 h at room temperature. After washing with TTBS, the blot was visualized using the ECL system.

Immunofluorescence localization

Formalin-fixed mouse lung left lobes were dehydrated gradually in ethanol, embedded in paraffin, and cut into 5 μm sections and heat-induced epitope retrieval was performed before staining. The tissues were permeabilized with 0.2% Triton X-100 for 10 min and blocked with phosphate-buffered saline (PBS) containing 1% BSA and 10% normal goat serum. We then double stained with anti-SP-C and anti-DUOX2 antibodies or anti-VWF and anti-DUOX2 antibodies. After extensive washing with PBS, tissues were treated with Alexa568-conjugated anti-rabbit IgG and Alexa488-conjugated anti-goat IgG or Alexa568-conjugated anti-rabbit IgG and Alexa488-conjugated anti-mouse IgG. Co-localization of SP-C and DUOX2 or VWF and DUOX2 was analyzed by confocal microscopy (Carl Zeiss; LSM 700). For sections of fixed lung, tissue was treated with anti-fibrin antibody or anti-cleaved caspase3 antibody and examined using confocal microscopy.

BAL fluid collection

BAL fluid (BALF) was obtained from mouse lungs using 0.5 ml PBS after cannulation of the trachea. The collected BALF was centrifuged at 1000 *g* for 10 min. The cell pellet was deposited onto glass slides using a Cytospin centrifuge (600 *g* for 5 min) and used for differential cell counts by staining with a Diff-Quik Stain Set. The supernatant was collected and stored at -20°C or -80°C for BAL protein assays and LDH activity, respectively.

Assessment of lung injury

BAL protein was measured using a protein quantification assay (Pierce BCA Protein Assay) on BALF supernatant according to the manufacturer's instructions. Evans Blue Dye assay was performed as previously described (39). In brief, Evans Blue (Sigma-Aldrich; 30 mg/kg) was injected intraperitoneally and allowed to circulate for 2 h before mice were sacrificed. At the time of sacrifice, blood was sampled by heart puncture and centrifuged at 1600 *g* for 5 min to collect the plasma. Subsequently, lungs were perfused with PBS through the right ventricle to remove intravascular dye from the lung. Lungs were placed in 1 ml of formamide followed by incubation for 16 h at 60°C, and the absorption of Evans Blue was measured spectrophotometrically at a wavelength of 620 nm. Vascular leakage was expressed as OD_{620}/gram of lung weight. IgM levels in BAL fluid samples were measured using a murine-specific IgM ELISA kit (Bethyl Laboratories).

Measurement of cell death

LDH activity was measured in BAL supernatant as previously described (14). BALF supernatant was measured at 490 nm using an LDH determination kit according to the manufacturer's instructions (Promega). For sections of fixed lung, DNA fragmentation and cell death were evaluated by terminal deoxynucleotidyl transferase (TdT)-mediated dUTP nick end labeling (TUNEL) assay. TUNEL was performed with an *in situ* Cell Death Detection Kit (Fluorescein, Roche) according to the manufacturer's protocol.

Isolation and culture of mouse type II AECs

Type II AECs were isolated from adult mice (9–14 weeks old) lungs as described with slight modifications (15). In brief, mice were anesthetized using a mixture of Zoletil and Rompun, and the lungs were perfused with PBS. The trachea was cannulated, and 2 ml of dispase (BD Biosciences) was instilled followed immediately by 1 ml of 1% low-melt agarose. The lung was placed in ice-cold PBS for 2 min. Lungs were removed, immersed in 2 ml of dispase, incubated for 45 min at room temperature, and then minced in growth medium containing 0.01% DNase. The cell suspension was then filtered consecutively through 100-μm and then 40-μm cell strainers (BD Biosciences). Single-cell suspensions were centrifuged at 1200 rpm for 5 min, resuspended in DMEM + 10% FBS, and incubated on anti-CD45- and anti-CD16/32- (clones 30-F11, 93, eBioscience)-coated plates for 2 h. Nonadhered cells were cultured directly on matrigel-coated cell culture plates in the presence of Keratinocyte Growth Factor (KGF, 10 ng/ml). Cells were cultured for approximately 5 days, and the media were exchanged every 2 days.

Murine transformed lung epithelial cell culture

Murine transformed lung epithelial cells (MLE12; American Type Culture Collection) were maintained in Dulbecco's modified Eagle's medium (DMEM; Life Technologies) supplemented with 10% fetal bovine serum and 1% penicillin/streptomycin. Cells were cultured at 37°C in a humidified atmosphere containing 5% CO_2. All experiments were conducted in confluent and quiescent cells in a monolayer to avoid cell density variability.

DUOX1 and DUOX2, NOX1 silencing using siRNA and lentiviral shRNA in MLE12 cells and mouse lung epithelia

For DUOX1 and DUOX2 silencing in MLE12 cells, cells were transfected with control siRNA, DUOX1 siRNA (5′-GAGACAAAGUGAGAAUUAAUU-3′), and DUOX2 siRNA (5′-CAAAGAGAGUCUGAAGAAAUU-3′) purchased from Genolution Pharmaceuticals. NOX1 siRNA (number: 1392760) were purchased from Bioneer. For DUOX2 and NOX1 silencing in mouse lung epithelia using shRNA lentivirus particles (Thermo Scientific), mice were anesthetized with 50 mg/kg Zoletil (Virbac) and 10 mg/kg Rompun (Bayer AG) and given either mouse Duox2 shRNA (cloneID: V3LMM-425530), NOX1 shRNA (cloneID: V2LMM_33862) or scrambled shRNA lentiviral particles (3×10^7 TU/ml) intranasally in a total volume of 30ul. After 6 days, the mice were used for the experiments.

DUOX2 overexpression using full length of cDNA clones in MLE12 cells

For DUOX2 overexpression in MLE12 cells, cells were transfected with mouse DUOX2 cDNA clone purchased from Origene.

Real time-PCR

Total RNA was isolated from MLE12 cells using TRIzol (Invitrogen). cDNA was synthesized from 1 μg RNA with random hexamer primers using Moloney murine leukemia virus reverse transcriptase (Applied Biosystems). To quantify gene expression, fluorescence real-time PCR was executed using the SYBR Green qPCR kit (Kapa Biosystems). Primer pairs for real-time PCR were designed and manufactured by Bioneer. The unique primer sequences of the target genes were as follows: β-actin (sense: 5′-TCA CCC ACA CTG TGC CCA TCT ACG A-3′, antisense: 5′-GGA TGC CAC AGG ATT CCA TAC CCA-3′), Nox1 (sense: 5′-AGG TCG TGA TTA CCA AGG TTG TC -3′, antisense: 5′-AAG CCT CGC TTC CTC ATC TG -3′), Nox2 (sense: 5′-AGC TAT GAG GTG GTG ATG TTA GTG G -3′, antisense: 5′-CAC AAT ATT TGT ACC AGA CAG ACT TGA G -3′), Nox4 (sense: 5′-CCC AAG TTC CAA GCT CAT TTC C -3′, antisense: 5′-TGG TGA CAG GTT TGT TGC TCC T -3′), Duox1 (sense: 5′-TAC ATC AGC CAG GAG AAG ATC TGC -3′, antisense: 5′-TGC GTT GAA ACT TCT CTC GGT GTG -3′), and Duox2 (Sense: 5′-TCC ATT AGT GAG TCT GAT TGT C-3′, antisense: 5′-GTT TGT CAA GGA CCT GCA GAC T-3′). Real-time PCR was performed using the PE Biosystems ABI PRISM® 7300 sequence detection system. The thermocycling parameters were 50°C for 2 min and 95°C for 20 s, followed by 40 cycles of 95°C for 3 s and 60°C for 30 s. All reactions were performed in triplicate. The relative quantity of mRNA was determined using the comparative threshold method, and the results were normalized against β-actin as an endogenous control.

Intracellular ROS assay by DCF-DA or DHA

After exposing the confluent cells to hyperoxia, the cells were washed with Hanks' balanced salt solution (HBSS) and incubated for 10 min at 37°C in an incubator in the dark in HBSS containing 20 μM 2′,7′-dichlorodihydrofluorescein diacetate (DCF-DA) (Molecular Probes) to detect intracellular hydrogen peroxide and 10 μM DHE (Sigma) to detect intracellular superoxide, respectively. Inside the cell, DCF-DA is converted into 2′7′- DCF by intracellular esterases and then oxidized to highly fluorescent 2′7′-DCF by reacting with hydrogen peroxide and DHE is converted to 2-hydroxyethidium (2-OH-E^+) or a precursor by reacting with superoxide. The cells were washed with 1 ml of HBSS at one time to remove extracellular ROS. Culture dishes filled with 1 ml of fresh HBSS were examined with a Zeiss LSM 700 laser confocal microscope that was equipped with 10× and 20× objectives. DCF fluorescence was measured at an excitation wavelength of 488 nm and an emission wavelength of 515–540 nm.

DHE fluorescence was measured at an excitation wavelength of 488 nm and an emission wavelength of 585 nm. The fluorescences were visualized with an image size of 512×512 pixels, getting an average of 8 image frames with fast scanning speed. The mean fluorescence intensity of DCF and DHE was assessed by selecting randomly at least six fields of each dish using ZEN 2012 (Carl zeiss) software.

MLE12 cells were treated with BAPTA AM (10 μM) for 30 min and exposed to hyperoxia, and BAPTA-AM (30 μM) was treated to ATII cells for 30 min, in addition, just before measuring ROS.

Flow cytometry

Cells were trypsinized, washed with HBSS containing 1% FBS, and stained with anti-SP-C and anti-AQP5 antibodies for 30 min at room temperature. After washing with HBSS containing 1% FBS, cells were incubated with Alexa647-conjugated anti-rabbit IgG and Alexa488-conjugated anti-goat IgG for 30 min at room temperature. After washing twice with HBSS containing 1% FBS, flow cytometry was performed. To detect apoptosis, cells were stained with Annexin V-FITC and active caspase3-FITC using Annexin V FITC apoptosis kit and caspase3 active form apoptosis kit, respectively. Data were acquired and analyzed with a BD LSRII flow cytometer (BD biosciences).

Statistical analyses

Results are presented as the mean of three determinations ± SEM. Wilcoxon rank-sum test was performed to determine differences between groups using R version 3.0.1 program (The R foundation for statistical computing, Vienna, Austria). p-values less than 0.05 were considered statistically significant.

Acknowledgments

The authors thank Yonsi-Carl Zeiss Advanced Imaging Center, Yonsei University College of Medicine, for technical assistance. They thank D.S. Jang for his excellent support with medical illustration. This research was supported by the Basic Science Research Program through the National Research Foundation of Korea (NRF) funded by the Ministry of Education (2013R1A1A200), by the Yonsei University College of Medicine (6-2012-0137 to J.-H.R.), by an NRF grant funded by the Korean government (MSIP) (No. 2007-0056092), and by an NRF grant funded by the Ministry of Science, ICT & Future Planning (2012M3A9C5048709), (NRF-2013M3A9D5072551).

Author Disclosure Statement

No competing financial interests exist.

References

1. Aderibigbe AO, Thomas RF, Mercer RR, and Auten RL, Jr. Brief exposure to 95% oxygen alters surfactant protein D and mRNA in adult rat alveolar and bronchiolar epithelium. *Am J Respir Cell Mol Biol* 20: 219–227, 1999.
2. Ameziane-El-Hassani R, Morand S, Boucher JL, Frapart YM, Apostolou D, Agnandji D, Gnidehou S, Ohayon R, Noel-Hudson MS, Francon J, Lalaoui K, Virion A, and Dupuy C. Dual oxidase-2 has an intrinsic Ca2+-dependent H2O2-generating activity. *J Biol Chem* 280: 30046–30054, 2005.
3. Babior BM. The leukocyte NADPH oxidase. *Isr Med Assoc J* 4: 1023–1024, 2002.
4. Bae YS, Choi MK, and Lee WJ. Dual oxidase in mucosal immunity and host-microbe homeostasis. *Trends Immunol* 31: 278–287, 2010.
5. Berry DD, Pramanik AK, Philips JB, 3rd, Buchter DS, Kanarek KS, Easa D, Kopelman AE, Edwards K, and Long W. Comparison of the effect of three doses of a synthetic surfactant on the alveolar-arterial oxygen gradient in infants weighing > or = 1250 grams with respiratory distress

syndrome. American Exosurf Neonatal Study Group II. *J Pediatr* 124: 294–301, 1994.
6. Boots AW, Hristova M, Kasahara DI, Haenen GR, Bast A, and van der Vliet A. ATP-mediated activation of the NADPH oxidase DUOX1 mediates airway epithelial responses to bacterial stimuli. *J Biol Chem* 284: 17858–17867, 2009.
7. Brown DI and Griendling KK. Nox proteins in signal transduction. *Free Radic Biol Med* 47: 1239–1253, 2009.
8. Caillou B, Dupuy C, Lacroix L, Nocera M, Talbot M, Ohayon R, Deme D, Bidart JM, Schlumberger M, and Virion A. Expression of reduced nicotinamide adenine dinucleotide phosphate oxidase (ThoX, LNOX, Duox) genes and proteins in human thyroid tissues. *J Clin Endocrinol Metab* 86: 3351–3358, 2001.
9. Carnesecchi S, Deffert C, Donati Y, Basset O, Hinz B, Preynat-Seauve O, Guichard C, Arbiser JL, Banfi B, Pache JC, Barazzone-Argiroffo C, and Krause KH. A key role for NOX4 in epithelial cell death during development of lung fibrosis. *Antioxid Redox Signal* 15: 607–619, 2011.
10. Carnesecchi S, Deffert C, Pagano A, Garrido-Urbani S, Metrailler-Ruchonnet I, Schappi M, Donati Y, Matthay MA, Krause KH, and Barazzone Argiroffo C. NADPH oxidase-1 plays a crucial role in hyperoxia-induced acute lung injury in mice. *Am J Respir Crit Care Med* 180: 972–981, 2009.
11. Carnesecchi S, Pache JC, and Barazzone-Argiroffo C. NOX enzymes: potential target for the treatment of acute lung injury. *Cell Mol Life Sci* 69: 2373–2385, 2012.
12. Chang S, Linderholm A, Franzi L, Kenyon N, Grasberger H, and Harper R. Dual oxidase regulates neutrophil recruitment in allergic airways. *Free Radic Biol Med* 65C: 38–46, 2013.
13. Chowdhury AK, Watkins T, Parinandi NL, Saatian B, Kleinberg ME, Usatyuk PV, and Natarajan V. Src-mediated tyrosine phosphorylation of p47phox in hyperoxia-induced activation of NADPH oxidase and generation of reactive oxygen species in lung endothelial cells. *J Biol Chem* 280: 20700–20711, 2005.
14. Chu SJ, Perng WC, Hung CM, Chang DM, Lin SH, and Huang KL. Effects of various body temperatures after lipopolysaccharide-induced lung injury in rats. *Chest* 128: 327–336, 2005.
15. Corti M, Brody AR, and Harrison JH. Isolation and primary culture of murine alveolar type II cells. *Am J Respir Cell Mol Biol* 14: 309–315, 1996.
16. El Hassani RA, Benfares N, Caillou B, Talbot M, Sabourin JC, Belotte V, Morand S, Gnidehou S, Agnandji D, Ohayon R, Kaniewski J, Noel-Hudson MS, Bidart JM, Schlumberger M, Virion A, and Dupuy C. Dual oxidase2 is expressed all along the digestive tract. *Am J Physiol Gastrointest Liver Physiol* 288: G933–G942, 2005.
17. Fischer H. Mechanisms and function of DUOX in epithelia of the lung. *Antioxid Redox Signal* 11: 2453–2465, 2009.
18. Fischer H, Gonzales LK, Kolla V, Schwarzer C, Miot F, Illek B, and Ballard PL. Developmental regulation of DUOX1 expression and function in human fetal lung epithelial cells. *Am J Physiol Lung Cell Mol Physiol* 292: L1506–L1514, 2007.
19. Forteza R, Salathe M, Miot F, Forteza R, and Conner GE. Regulated hydrogen peroxide production by Duox in human airway epithelial cells. *Am J Respir Cell Mol Biol* 32: 462–469, 2005.
20. Gattas MV, Forteza R, Fragoso MA, Fregien N, Salas P, Salathe M, and Conner GE. Oxidative epithelial host defense is regulated by infectious and inflammatory stimuli. *Free Radic Biol Med* 47: 1450–1458, 2009.
21. Geiszt M, Witta J, Baffi J, Lekstrom K, and Leto TL. Dual oxidases represent novel hydrogen peroxide sources supporting mucosal surface host defense. *FASEB J* 17: 1502–1504, 2003.
22. Griffith B, Pendyala S, Hecker L, Lee PJ, Natarajan V, and Thannickal VJ. NOX enzymes and pulmonary disease. *Antioxid Redox Signal* 11: 2505–2516, 2009.
23. Harper RW, Xu C, Eiserich JP, Chen Y, Kao CY, Thai P, Setiadi H, and Wu R. Differential regulation of dual NADPH oxidases/peroxidases, Duox1 and Duox2, by Th1 and Th2 cytokines in respiratory tract epithelium. *FEBS Lett* 579: 4911–4917, 2005.
24. Hecker L, Vittal R, Jones T, Jagirdar R, Luckhardt TR, Horowitz JC, Pennathur S, Martinez FJ, and Thannickal VJ. NADPH oxidase-4 mediates myofibroblast activation and fibrogenic responses to lung injury. *Nat Med* 15: 1077–1081, 2009.
25. Johnson KR, Marden CC, Ward-Bailey P, Gagnon LH, Bronson RT, and Donahue LR. Congenital hypothyroidism, dwarfism, and hearing impairment caused by a missense mutation in the mouse dual oxidase 2 gene, Duox2. *Mol Endocrinol* 21: 1593–1602, 2007.
26. Joo JH, Ryu JH, Kim CH, Kim HJ, Suh MS, Kim JO, Chung SY, Lee SN, Kim HM, Bae YS, and Yoon JH. Dual oxidase 2 is essential for the toll-like receptor 5-mediated inflammatory response in airway mucosa. *Antioxid Redox Signal* 16: 57–70, 2012.
27. Koff JL, Shao MX, Ueki IF, and Nadel JA. Multiple TLRs activate EGFR via a signaling cascade to produce innate immune responses in airway epithelium. *Am J Physiol Lung Cell Mol Physiol* 294: L1068–L1075, 2008.
28. Lambeth JD, Kawahara T, and Diebold B. Regulation of Nox and Duox enzymatic activity and expression. *Free Radic Biol Med* 43: 319–331, 2007.
29. Lee PJ and Choi AM. Pathways of cell signaling in hyperoxia. *Free Radic Biol Med* 35: 341–350, 2003.
30. Leto TL and Geiszt M. Role of Nox family NADPH oxidases in host defense. *Antioxid Redox Signal* 8: 1549–1561, 2006.
31. Li J, Gao X, Qian M, and Eaton JW. Mitochondrial metabolism underlies hyperoxic cell damage. *Free Radic Biol Med* 36: 1460–1470, 2004.
32. Mantell LL, Horowitz S, Davis JM, and Kazzaz JA. Hyperoxia-induced cell death in the lung—the correlation of apoptosis, necrosis, and inflammation. *Ann N Y Acad Sci* 887: 171–180, 1999.
33. Min JH, Codipilly CN, Nasim S, Miller EJ, and Ahmed MN. Synergistic protection against hyperoxia-induced lung injury by neutrophils blockade and EC-SOD overexpression. *Respir Res* 13: 58, 2012.
34. Parinandi NL, Kleinberg MA, Usatyuk PV, Cummings RJ, Pennathur A, Cardounel AJ, Zweier JL, Garcia JG, and Natarajan V. Hyperoxia-induced NAD(P)H oxidase activation and regulation by MAP kinases in human lung endothelial cells. *Am J Physiol Lung Cell Mol Physiol* 284: L26–L38, 2003.
35. Pendyala S, Gorshkova IA, Usatyuk PV, He D, Pennathur A, Lambeth JD, Thannickal VJ, and Natarajan V. Role of Nox4 and Nox2 in hyperoxia-induced reactive oxygen species generation and migration of human lung endothelial cells. *Antioxid Redox Signal* 11: 747–764, 2009.

36. Pendyala S, Moitra J, Kalari S, Kleeberger SR, Zhao Y, Reddy SP, Garcia JG, and Natarajan V. Nrf2 regulates hyperoxia-induced Nox4 expression in human lung endothelium: identification of functional antioxidant response elements on the Nox4 promoter. *Free Radic Biol Med* 50: 1749–1759, 2011.
37. Rada B and Leto TL. Characterization of hydrogen peroxide production by Duox in bronchial epithelial cells exposed to Pseudomonas aeruginosa. *FEBS Lett* 584: 917–922, 2010.
38. Reddy NM, Kleeberger SR, Kensler TW, Yamamoto M, Hassoun PM, and Reddy SP. Disruption of Nrf2 impairs the resolution of hyperoxia-induced acute lung injury and inflammation in mice. *J Immunol* 182: 7264–7271, 2009.
39. Reddy NM, Potteti HR, Mariani TJ, Biswal S, and Reddy SP. Conditional deletion of Nrf2 in airway epithelium exacerbates acute lung injury and impairs the resolution of inflammation. *Am J Respir Cell Mol Biol* 45: 1161–1168, 2011.
40. Reddy SP, Hassoun PM, and Brower R. Redox imbalance and ventilator-induced lung injury. *Antioxid Redox Signal* 9: 2003–2012, 2007.
41. Romashko J, 3rd, Horowitz S, Franek WR, Palaia T, Miller EJ, Lin A, Birrer MJ, Scott W, and Mantell LL. MAPK pathways mediate hyperoxia-induced oncotic cell death in lung epithelial cells. *Free Radic Biol Med* 35: 978–993, 2003.
42. Ryu JH, Yoo JY, Kim MJ, Hwang SG, Ahn KC, Ryu JC, Choi MK, Joo JH, Kim CH, Lee SN, Lee WJ, Kim J, Shin DM, Kweon MN, Bae YS, and Yoon JH. Distinct TLR-mediated pathways regulate house dust mite-induced allergic disease in the upper and lower airways. *J Allergy Clin Immunol* 131: 549–561, 2013.
43. Sanders SP, Zweier JL, Kuppusamy P, Harrison SJ, Bassett DJ, Gabrielson EW, and Sylvester JT. Hyperoxic sheep pulmonary microvascular endothelial cells generate free radicals via mitochondrial electron transport. *J Clin Invest* 91: 46–52, 1993.
44. Usatyuk PV, Romer LH, He D, Parinandi NL, Kleinberg ME, Zhan S, Jacobson JR, Dudek SM, Pendyala S, Garcia JG, and Natarajan V. Regulation of hyperoxia-induced NADPH oxidase activation in human lung endothelial cells by the actin cytoskeleton and cortactin. *J Biol Chem* 282: 23284–23295, 2007.
45. van der Vliet A. NADPH oxidases in lung biology and pathology: host defense enzymes, and more. *Free Radic Biol Med* 44: 938–955, 2008.
46. van Klaveren RJ, Roelant C, Boogaerts M, Demedts M, and Nemery B. Involvement of an NAD(P)H oxidase-like enzyme in superoxide anion and hydrogen peroxide generation by rat type II cells. *Thorax* 52: 465–471, 1997.
47. Wang D, De Deken X, Milenkovic M, Song Y, Pirson I, Dumont JE, and Miot F. Identification of a novel partner of duox: EFP1, a thioredoxin-related protein. *J Biol Chem* 280: 3096–3103, 2005.
48. Ware LB and Matthay MA. The acute respiratory distress syndrome. *N Engl J Med* 342: 1334–1349, 2000.
49. Waxman AB, Einarsson O, Seres T, Knickelbein RG, Warshaw JB, Johnston R, Homer RJ, and Elias JA. Targeted lung expression of interleukin-11 enhances murine tolerance of 100% oxygen and diminishes hyperoxia-induced DNA fragmentation. *J Clin Invest* 101: 1970–1982, 1998.
50. Yue DM and Xue XD. [Relationship between expression of aquaporin-1, -5 and pulmonary edema in hyperoxia-induced lung injury in newborn rats]. *Zhongguo Dang Dai Er Ke Za Zhi* 8: 147–150, 2006.
51. Zhang X, Shan P, Sasidhar M, Chupp GL, Flavell RA, Choi AM, and Lee PJ. Reactive oxygen species and extracellular signal-regulated kinase 1/2 mitogen-activated protein kinase mediate hyperoxia-induced cell death in lung epithelium. *Am J Respir Cell Mol Biol* 28: 305–315, 2003.

Address correspondence to:
Dr. Ji-Hwan Ryu
Research Center for Natural Human Defense System
Yonsei University College of Medicine
50 Yonsei-ro, Seodaemun-gu
Seoul 120-752
Korea

E-mail: yjh@yuhs.ac

Date of first submission to ARS Central, October 4, 2013; date of final revised submission, April 8, 2014; date of acceptance, April 26, 2014.

Abbreviations Used

AEC = alveolar epithelial cell
ALI = acute lung injury
BAL = bronchoalveolar lavage
BALF = bronchoalveolar lavage fluid
DAPI = 4′,6-diamidino-2-phenylindole
DCF = dichlorodihydrofluorescein
DHE = dihydroethidium
DMEM = Dulbecco's modified Eagle's medium
DUOX2 = dual oxidase2
EBD = evans blue dye
HBSS = Hanks' balanced salt solution
IgM = immunoglobulin M
IHC = immunohistochemical
LDH = lactate dehydrogenase
MAPK = mitogen-activated protein kinase
MLE12 = murine transformed lung epithelial 12
NAC = N-acetylcysteine
NOX = NADPH oxidase
NRF2 = NF-E2-related factor 2
PBS = phosphate-buffered saline
RA = room air
ROS = reactive oxygen species
SOD = superoxide dismutase
SP-C = surfactant protein-c
TUNEL = terminal deoxynucleotidyl transferase (TdT)-mediated dUTP nick end labeling
VWF = von Willebrand factor
WT = wild type